JTTEE5 11:107-118

Numerical Study of the Relative Importance of Turbulence, Particle Size and Density, and Injection Parameters on Particle Behavior During Thermal Plasma Spraying

R.L. Williamson, J.R. Fincke, and C.H. Chang

(Submitted 6 October 2000; in revised form 4 January 2001)

Numerical modeling is used to systematically examine the effects of turbulence, injection, and particle characteristics on particle behavior during thermal plasma spraying. Using the computer program LAVA (Idaho National Engineering and Environmental Laboratory, Idaho Falls, ID), a steady-state plasma jet typical of a commercial torch at normal operating conditions is first developed. Then, assuming a single particle composition (ZrO_2) and injection location, real world complexity (e.g., turbulent dispersion, particle size and density, injection velocity, and direction) is introduced "one phenomenon at a time" to distinguish and characterize its effect and enable comparisons of separate effects. A final calculation then considers all phenomena simultaneously, to enable further comparisons. Investigating each phenomenon separately provides valuable insight into particle behavior. For the typical plasma jet and injection conditions considered, particle dispersion in the injection direction is most significantly affected by (in order of decreasing importance): particle size distribution, injection velocity distribution, turbulence, and injection direction distribution or particle density distribution. Only the distribution of injection directions and turbulence affect dispersion normal to the injection direction and are of similar magnitude in this study. With regards to particle velocity and temperature, particle size is clearly the dominant effect.

Keywords feeding, feedstock, injection parameters, turbulence

1. Introduction

The use of plasma spraying to modify surfaces has developed into an important manufacturing process, with many industrial applications.[1-4] To gain widespread industrial acceptance, however, improvements are needed both in coating quality and reproducibility. Clearly, a better understanding of the plasma spray process will lead to such improvements.

Plasma spray technology is highly complex, with many variables affecting the final product. As described by Vardelle et al.,[5] these variables can be categorized in terms of five subsystems[6-8] over which some design or operator control can be exercised: (a) the plasma jet, which depends on torch geometry, gas composition and flow rates, and arc power; (b) the powder composition, morphology, size and density distributions, the particle injection location, velocity and direction, and the carrier-gas flow rate; (c) the composition and properties of the enveloping atmosphere; (d) the physical and chemical characteristics of the target as well as its distance from the plasma torch exit; and (e) the motion of the torch relative to the target.

The objective of this study is to use numerical modeling to systematically examine a few of the preceding variables listed. Specifically, the effects of turbulent dispersion, distributions in particle size and density, and distributions in injection velocity and direction are considered. In this context, a computational approach clearly has advantages over a purely experimental investigation. Computationally, the relative importance of each variable can be examined separately in a controlled manner, a process that, experimentally, is virtually impossible.

LAVA, a computer program specifically designed for analyzing thermal plasmas containing entrained particles, will be used for the study. The approach will be to first develop a steady-state plasma jet typical of a commercial torch at normal operating conditions. Then, assuming a single particle composition (ZrO_2) and injection location, real world complexity (e.g., turbulent dispersion, particle size distribution, etc.) will be introduced "one phenomenon at a time" to distinguish and characterize its effect, enable comparisons of separate effects, and investigate how each adds to the combined result.

R.L. Williamson and **J.R. Fincke,** Idaho National Engineering and Environmental Laboratory, Idaho Falls, ID 83415-2218; and **C.H. Chang,** Los Alamos National Laboratory, University of California, Los Alamos, NM 87545. Contact e-mail: rlw@inel.gov.

2. LAVA Background

LAVA is a fluid dynamics software program for simulating thermal plasmas containing entrained particles in the absence of electromagnetic fields. The computer program has been under continuous development at the Idaho National Engineering and Environmental Laboratory for approximately the last decade. The LAVA program is being developed primarily for plasma spray applications, with a particular emphasis on plasma jets. A fluid-particle approach is employed, similar to that used previously to model fuel sprays in internal combustion engines.[9-11]

In LAVA, the plasma is represented as a continuous, multicomponent, chemically reacting ideal gas, governed by the complete transient compressible Navier-Stokes equations in two or three dimensions. Temperature-dependent thermodynamic and transport properties are included. Turbulence is approximated by either subgrid-scale or k-ε models. Species diffusion is calculated by an effective binary-diffusion approximation, which has been generalized to allow for ambipolar diffusion of charged species. Ionization, dissociation, recombination, and other chemical relations are simulated using general kinetic and equilibrium chemistry algorithms. The plasma is presumed to be optically thin; thus, radiative heat loss is modeled as a simple temperature-dependent volumetric sink term. Detailed descriptions of the fluid dynamics aspects of LAVA have been given previously.[12,13]

Particles are modeled as discrete Lagrangian entities, which exchange momentum and energy with the plasma. The concept of a "computational particle" is employed, where each computational particle is representative of a group of similar real particles. Computational particles are stochastically generated by sampling from probability distributions of particle properties (e.g., size, density, injection velocity, and direction). The LAVA program can process multiple particle types (ceramic and metallic, for instance) and multiple injection locations simultaneously. Although recent development efforts have included particle conduction, evaporation, and condensation in LAVA,[14] for this study, only particle heating and melting are considered. Thus, the particles are assumed to be lumped thermal-capacitance entities. Dukowicz's statistical approach[9] is used to approximate particle dispersion by turbulent gas motions. All plasma-particle interactions are treated in a fully self-consistent manner. As with the plasma flow, detailed descriptions of the particle models in LAVA have been given previously.[14,15]

The governing equations for both the plasma flow and the entrained particles are solved using standard finite-difference techniques. Both transient and steady-state simulations are possible.

3. Model Description

3.1 Approach

The plasma spray system considered in this study is consistent with a Metco 9MB commercial torch (#732A anode, #63 cathode; Sulzer Metco, Inc., Westbury, NY) discharging into ambient air. The arc gas was assumed to be a mixture of argon and hydrogen at flow rates of 40 and 12 slm, respectively. The torch was assumed to operate at 600 A and 70 V with a thermal efficiency of 70%. The ZrO_2 particles were injected from a single fixed location external to the nozzle at a rate of 0.33 g/s. A particle melting temperature of 2950 K was assumed.

Because three-dimensional (3-D) flow calculations are extremely time consuming with LAVA, the model employed a pseudo 3-D approach, wherein the plasma flow was assumed to be axisymmetric and described in two-dimensional (2-D) cylindrical coordinates, while the Lagrangian particle field was fully 3-D. Interactions between the particles and plasma are, thus, calculated in a ring-shaped circumferential control volume. Note that this approach becomes invalid when the particle loading rate is high but provides an efficient way of modeling most plasma spray processes where the 3-D effects on the plasma jet produced by injected particles are relatively minor. Reasonable comparisons to experimental results, which will be reported in a separate paper, provide justification of this simplifed approach.

The effect of the particle carrier gas was not included in the study primarily because the complex 3-D interaction of the carrier gas with the plasma jet cannot be accurately modeled with a 2-D axisymmetric flow assumption. This assumption is supported by the 3-D calculations of Vardelle et al.[5] and Dussoubs,[16] which suggest that for external powder injection, the carrier gas has only a small effect on the plasma jet. Additionally, the influence of a coflowing jet on particle trajectory, spray pattern, and particle heating was recently experimentally studied by Fincke et al.[17] For external injection and typical carrier-gas flow rates, this study did not show any significant effects attributable to interactions between the carrier-gas jet and the plasma jet. Based on these results and observations, the modification of the plasma jet was assumed to be of secondary importance and will not be addressed further in this paper.

A steady plasma-flow field was needed to systematically investigate particle behavior. To this end, an initial 3 ms transient calculation was run involving only the plasma gas (no particles), during which essentially steady flow conditions were established. Particles were then introduced into this flow and tracked for an additional 5 ms of spray time, which was sufficient to establish good statistical results on particle behavior. During this time, a minimum of 3000 computational particles were injected and numerically tracked until exiting the computational domain.

3.2 Geometry and Computational Mesh

The geometry and computational mesh used in the simulations are shown in Fig. 1. The model considers only the plasma jet exiting the torch; thus, the flow inlet plane of the model corresponds to the face of the torch body. The computational region was 6 cm radially and 15 cm axially and was discretized using a 56×65 computational mesh. The torch nozzle radius of 0.39 cm was represented by the leftmost 10 cells at the bottom boundary of the mesh. In all simulations, particle injection occurred at a point 0.6 cm downstream from the torch exit plane and 0.8 cm from the axis of symmetry ($x = 0$, $y = 0.6$ cm, and $z = 0.8$ cm).

3.3 Boundary Conditions

The three boundary condition types employed in the model, namely, inflow, torch wall, and open, are also identified in Fig. 1. Each condition is described subsequently.

Because only the plasma jet was considered in the model, radial profiles of temperature, velocity, species densities, and turbulence parameters (k-ε) at the torch exit (or inlet to the flow model) are required as inflow boundary conditions. These profiles are constrained by the assumption of ionization equilibrium and the known arc-gas flow rates and torch power but are otherwise unknown. The typical approach with LAVA simulations is to assume forms for these profiles, subject to the mentioned constraints. The temperature and axial velocity profiles at the torch exit plane ($y = 0$) were, thus, assumed to have the forms

$$T = (T_0 - T_w)\left[1 - \left(\frac{r}{R_{\text{in}}}\right)^{n_T}\right] + T_w \qquad \text{(Eq 1)}$$

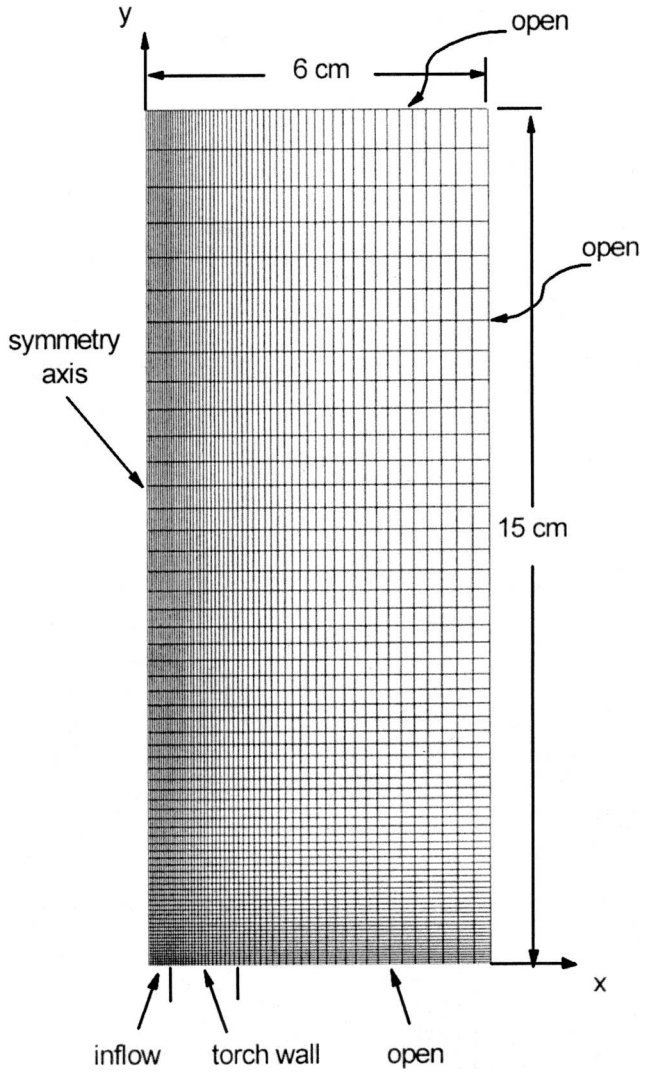

Fig. 1 The geometry, computational mesh, and boundary conditions used in the simulations

$$v = v_0\left[1 - \left(\frac{r}{R_{\text{in}}}\right)^{n_v}\right] \qquad \text{(Eq 2)}$$

where r is the radial coordinate, R_{in} is the torch nozzle exit radius, and T_w is the torch wall temperature. The centerline values, T_0 and v_0, and fitting parameters, n_T and n_v, were selected to match the known arc-gas flow rates and torch power as closely as possible, using the relations given in Eq. 51 and 52 of Ref 12. Experimental data were available for the torch considered in this study and were used to guide this selection. These measurements were obtained by a high-resolution laser-scattering technique,[18] which allows nonintrusive determination of both velocity and heavy particle (atom and ion) temperature. Axial velocity measurements along a radial profile 2 mm downstream from the torch face were well fit by Eq 2, using v_0 and n_v of 3370 m/s and 1.2, respectively. For this jet, temperature measurements were complicated by the presence of hydrogen, which broadens the measured scattered-light spectral profiles making exact determination of the temperature somewhat uncertain. The data suggest a centerline temperature of approximately 14,000 K with an uncertainty of ±10 to 15%. Values of 700 K and 6 were assumed for T_w and n_T, respectively. Because of the rapid mixing of the jet with the surrounding atmosphere, the calculation is not overly sensitive to centerline values of v_0 and T_0 used. The results are, however, somewhat more sensitive to the profile shape, which is determined by n_T and n_v. The value of n_T used is consistent with the known gas-mass flow rates and torch power. With the inlet temperature profile established, species density profiles were obtained by assuming ionization equilibrium and charge neutrality at ambient pressure. The radial velocity along the inflow boundary was assumed to be zero.

Information regarding inflow profiles of turbulence variables in plasma torches is not available. The inflow turbulent kinetic-energy profile was simply assumed to have the form[19]

$$k(r) = k_{\max}\left|\frac{\dfrac{\partial v}{\partial r}}{\left(\dfrac{\partial v}{\partial r}\right)_{\max}}\right| \qquad \text{(Eq 3)}$$

where $(\partial v/\partial r)_{\max}$ is the largest axial velocity gradient with respect to the radial direction at the torch exit, and $k_{\max}$ is defined as

$$k_{\max} = \frac{3}{2}(0.1v_0)^2 \qquad \text{(Eq 4)}$$

The inflow profile for ε was then obtained from the turbulent kinetic-energy profile by the prescription of Leschziner and Rodi.[20]

The torch face was treated as a solid boundary. Wall temperatures were assumed to vary between 700 K on the inside and 300 K on the outside, according to the following relation:

$$T = 700 - 400\frac{\ln\left(\dfrac{r}{R_{\text{in}}}\right)}{\ln\left(\dfrac{R_{\text{in}}}{R_{\text{out}}}\right)} \qquad \text{(Eq 5)}$$

where R_{in} and R_{out} are the inside and outside radii, respectively. This equation simply provides the steady-state radial temperature distribution for an annulus.

For the open boundaries, ambient pressure was assumed. Since the flow at these boundaries can be either outward or inward (entrainment), it was calculated rather than imposed. For outward flow, all other variables (including k and ε) were assigned a zero-gradient condition. For inward flow, the inflowing gas was assumed to be ambient temperature air ($k = \varepsilon = 0$) and assumed to enter the domain with a zero-gradient velocity in a direction normal to the boundary.

3.4 Particle Parametric Study

The key objective in this study, as described previously, was to better understand and quantify some of the factors affecting particle behavior. The basic approach was to begin with the sim-

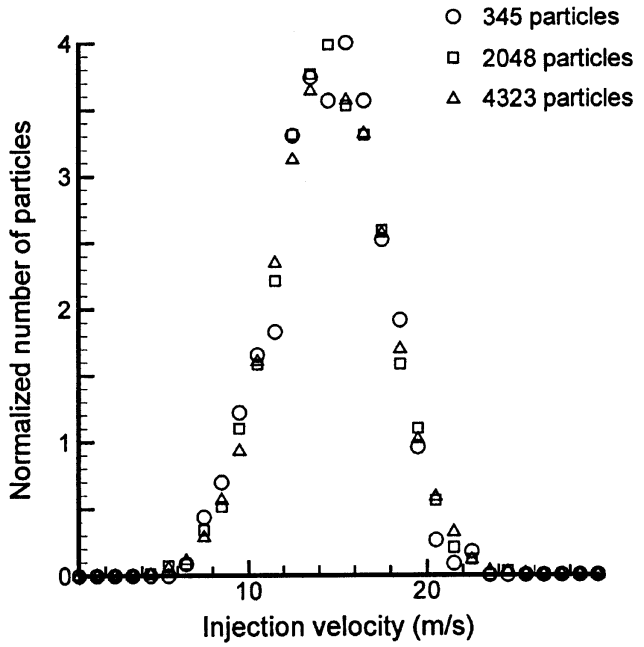

Fig. 2 The injection velocity distribution obtained in the simulations for various numbers of particles

Table 1 Summary of Cases Considered

Case	Turbulent Dispersion	Injection Velocity (m/s)	Injection Direction Cone Angle (°)	Particle Diameter (μm)	Particle Density (g/cm^3)
1	off	14.6	0	~50	5.89
2	on	14.6	0	~50	5.89
3	off	dist	0	~50	5.89
4	off	14.6	dist	~50	5.89
5	off	14.6	0	dist	5.89
6	off	14.6	0	~50	dist
7	on	dist	dist	dist	dist

plest case possible (a base case) and then add "real-world" complexity one phenomenon at a time. Table 1 presents a summary of this methodology and identifies each case considered.

Case 1 (the base case) assumed a fixed injection velocity (14.6 m/s) and direction ($-z$), with a constant particle density (5.89 g/cm^3) and nearly constant diameter (~50 μm). Turbulent dispersion was turned off. Cases 2 through 6 are then each identical to the base case, except for a single modification.

Note in Table 1 that the particle diameter is often listed as ~50 μm. The nature of the input structure to LAVA made it easiest to provide the particle size as a distribution rather than a single value. A nearly constant diameter was thus established by assuming a uniform distribution of particle sizes varying between 49 and 51 μm.

The particle turbulent-dispersion model was activated in case 2.

For case 3, the injection velocity of individual particles was prescribed such that the full set approximated a Gaussian distribution having an average value of 14.6 and a standard deviation of 3 m/s. This distribution was selected based on experimental

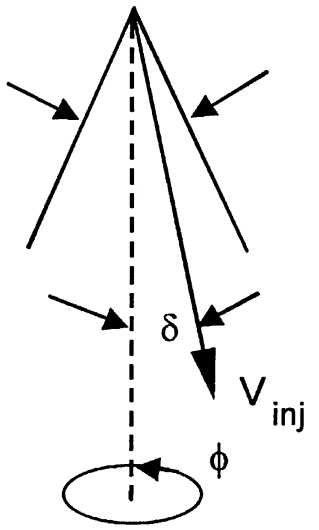

Fig. 3 Schematic showing the nomenclature used to specify particle injection directions

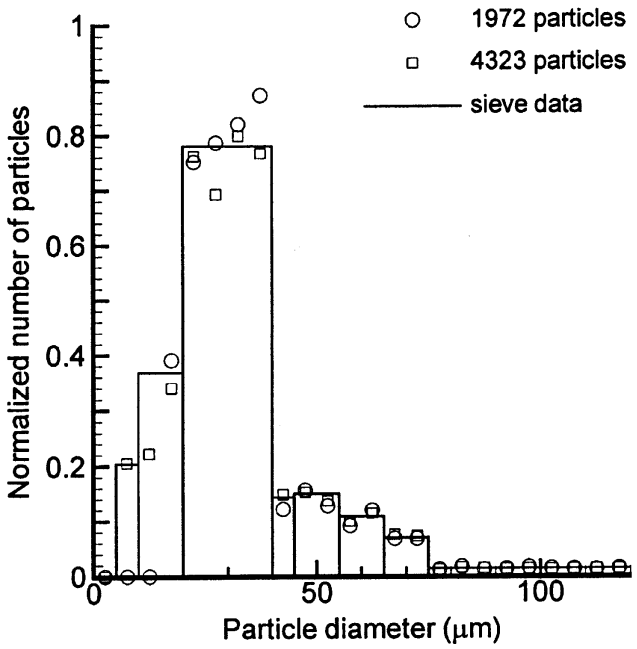

Fig. 4 The measured ZrO_2 particle-size distribution, as well as that achieved in the simulations

results.[21] The velocity distribution obtained for three different particle-set sizes, is shown in Fig. 2. The approximation obviously improves as the number of particles is increased, but the fit to a Gaussian distribution is very reasonable above 2000 particles.

A distribution was provided for the particle injection direction in case 4. Two angles were prescribed for each particle, as shown in Fig. 3. Angle δ was selected to provide a uniform random distribution over a cone angle of 20°, and angle ϕ provided a uniform random distribution over 360°. The 20° cone angle was selected based on experimental observations.

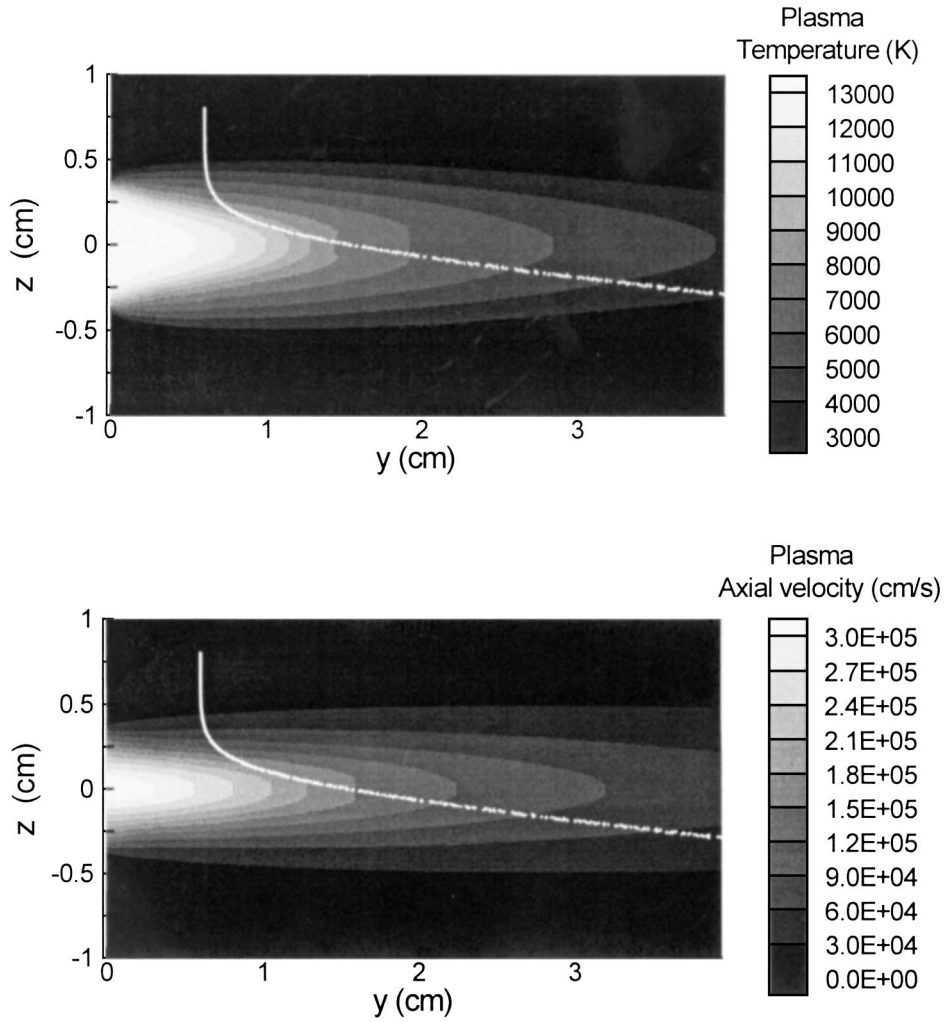

Fig. 5 The predicted steady-state temperature and axial velocity fields for the plasma jet, as well as calculated particle trajectory through the plasma, for case 1

In case 5, a particle size distribution was introduced based on sieve data for ZrO_2 particles.[21] The measured distribution, as well as that achieved in the simulation, are shown in Fig. 4. Again, for more than 2000 particles, the desired size distribution is reasonably well obtained.

Since experimental evidence indicates that particles can be porous, the effect of particle density was considered in case 6. For this calculation, the particle density was assumed to follow a uniform random distribution between 70% and full density. The particle mass injection rate was held constant.

For comparison purposes, a final calculation (case 7) was made where all effects were considered simultaneously.

4. Results and Discussion

4.1 Steady-State Plasma Flow Field and Base Case

The computed steady-state temperature and axial velocity fields for the plasma jet are shown in Fig. 5, as well as the particle field for the base case simulation (i.e., case 1). Very large temperature and velocity gradients exist in the plasma. The injection location and calculated particle trajectory through the plasma are evident. As expected for this simple case, the particles follow essentially a fixed trajectory with almost no dispersion.

In most of the results to follow, particle data are plotted for all particles passing through the *x*-*z* plane at an axial (*y*) distance of 10 cm from the torch face. This plane is of interest since it is a typical location for particle deposition. In the text that follows, this plane will simply be described as "at 10 cm from the torch face."

Figure 6 shows the predicted particle velocity and temperature as a function of particle diameter (recall that a uniform size distribution, 49 μm < D < 51 μm, was assumed) at 10 cm from the torch face. The line formed by the particles has a nonzero slope, indicating a particle size effect even over the narrow size distribution considered. The smaller particles achieve higher velocities and temperatures, as expected from flow drag and thermal mass considerations. The slight spread in the results for a given particle diameter is due to very small fluctuations in the plasma flow. For the geometry and flow conditions considered, the com-

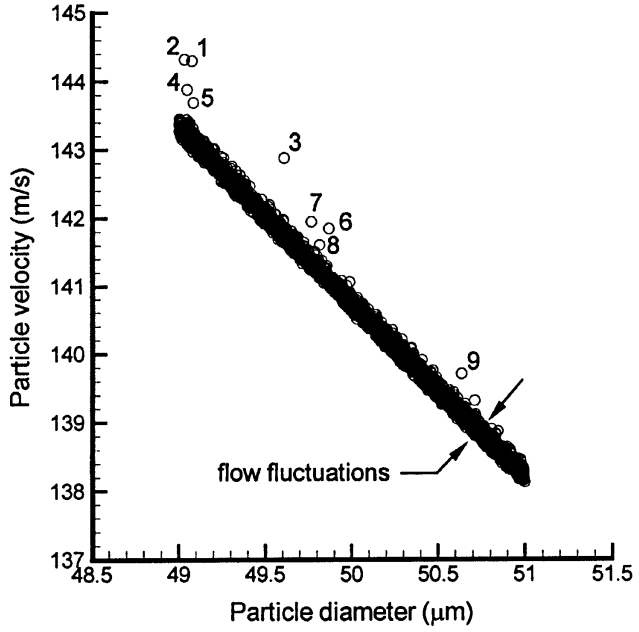

(a)

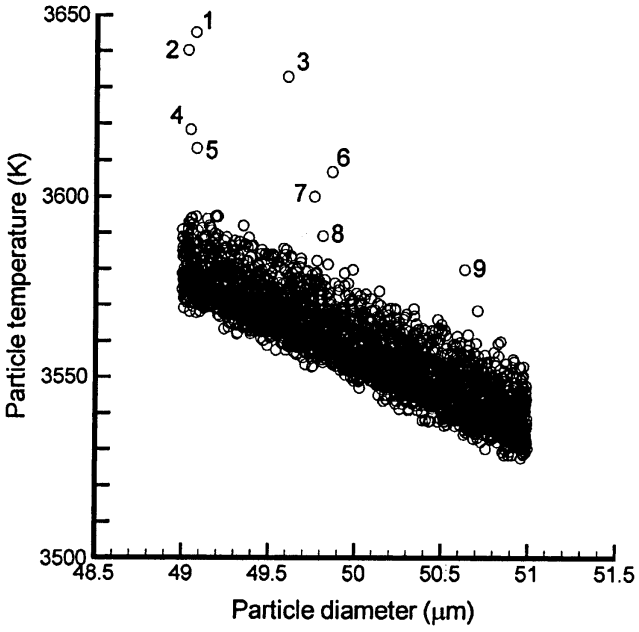

(b)

Fig. 6 The predicted **(a)** particle velocity and **(b)** temperature as a function of particle diameter at 10 cm from the torch face for case 1. Labels on individual particles denote the numerical order in which they were injected.

puted "steady-state" flow is never completely steady but exhibits a slight oscillation. A careful investigation to determine the source of this oscillation demonstrated it to be the result of an effort by the model to simulate an unsteady vortex near the torch face as the surrounding gas interacts with the plasma jet. Although neither the numerical scheme nor computational mesh are adequate to capture this phenomena accurately, small fluctuations are still observed in the results. Note that these oscillations are very small (e.g., centerline axial velocities vary by less than 2% of the mean in the region where particle-flow interaction occurs) and, as demonstrated in Fig. 6, have only a slight effect on the particle behavior.

Note in Fig. 6 that a few particles are above the general curve and appear to be some type of "noise" in the results. However, when individual particles are labeled in the order in which they were injected, as has been done in the figure, it is clear that only the first few particles fall outside the normal pattern. Note further that the difference in velocity or temperature between these particles and the norm generally drops with each new particle injected. Although these variations are slight, they are interesting and explainable. Since, in this simple case, all particles follow nearly the same trajectory, the first few particles locally slow and cool the plasma flow, leading to slight reductions in the velocity and temperature for subsequent particles.

4.2 Turbulent Dispersion

The effects of including turbulent dispersion in the model (i.e., case 2) are illustrated in Fig. 7, which shows the predicted spray pattern and particle velocity versus temperature relationship at 10 cm from the torch face. Results from the base case calculation are included for comparison. The spray pattern is essentially circular, as expected, with a diameter of approximately 5 mm. Particle temperatures vary over approximately 300 K and are reasonably well distributed both above and below the base case. Particle velocities vary over about 25 m/s but are not evenly distributed. This dispersion in temperature and velocity is strongly influenced by the radial velocity and temperature profiles of the plasma jet near the injection location. Recall from Eq 1 and 2 that the inflow velocity profile (n_v = 1.2) is much steeper than the temperature profile (n_t = 6). Any particle dispersed off the *y*-*z* plane enters a lower velocity and temperature region of the plasma jet; however, because of the steeper plasma-velocity profile, the effect on particle velocity is much more pronounced.

4.3 Injection Velocity

Figure 8 illustrates the effects of introducing a distribution in the particle injection velocity (i.e., case 3) and shows the predicted spray pattern and particle velocity versus temperature relationship at 10 cm from the torch face. Results from the base case calculation are included for comparison. Because all particles are injected in the same direction and in the *y*-*z* plane, there is no dispersion in *x*. There is, however, significant dispersion in *z*, with the particle field spread over approximately 1.5 cm. Since the injection direction is normal to the plasma flow, variations in injection velocity cause particles to traverse very different portions of the plasma jet. The width of the particle temperature band increases to approximately 1500 K, and the particle velocity band increases to about 40 m/s. Note in Fig. 8(b) that the particle temperatures reach a maximum at a particle velocity of approximately 140 m/s. Decreasing particle temperatures to the left of this peak correspond with lower injection velocities resulting in particles that do not pass through the highest tempera-

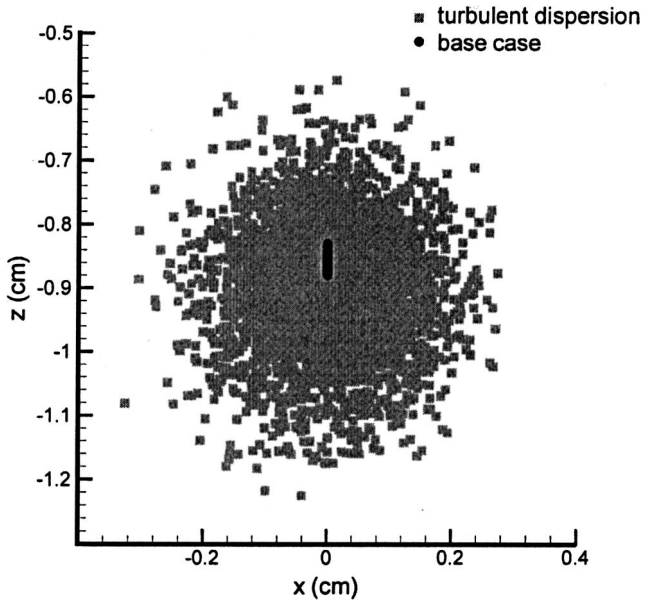

(a)

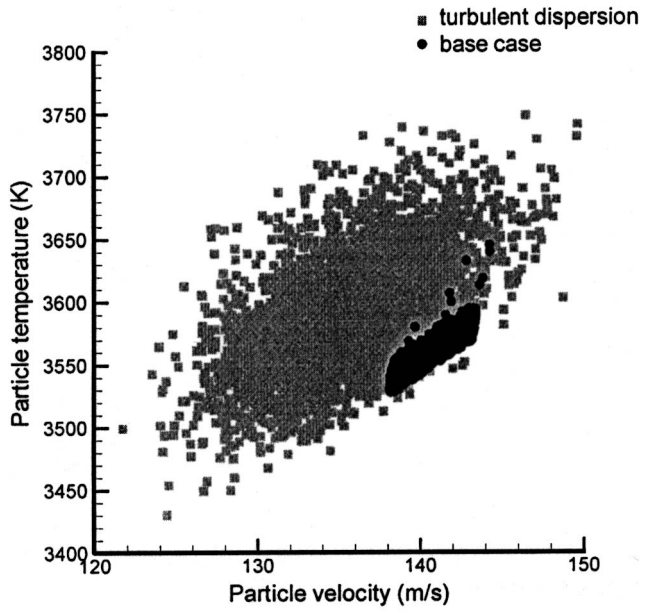

(b)

Fig. 7 The predicted **(a)** spray pattern and **(b)** particle velocity vs temperature relationship at 10 cm from the torch face, when turbulent dispersion (case 2) is included. Results from the base case calculation are also shown for comparison.

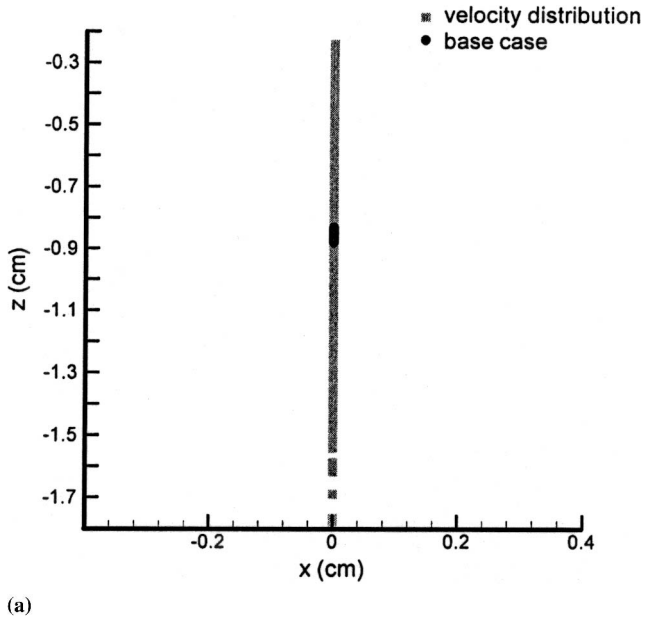

(a)

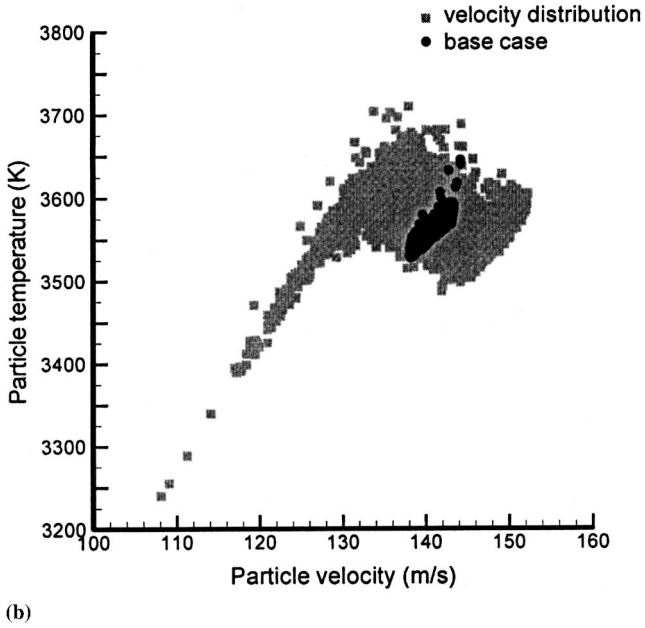

(b)

Fig. 8 The predicted **(a)** spray pattern and **(b)** particle velocity vs temperature relationship at 10 cm from the torch face, when a distribution in the particle injection velocity (case 3) is included. Results from the base case calculation are also shown for comparison.

ture region of the plasma jet. To the right of the peak, decreasing temperatures correspond to higher injection velocities and particles having shorter residence time in the highest temperature region of the jet.

4.4 Injection Direction

The effects of including a distribution in the particle injection direction (i.e., case 4) is illustrated in Fig. 9, which shows the predicted spray pattern and the particle velocity versus temperature relationship at 10 cm from the torch face. Base case results are again included for comparison. In this case, dispersion in the x-direction (~5 mm) is about twice that in z (~2.5 mm), and a concave spray pattern is formed. Since any particle injected off the y-z plane experiences a lower velocity region in the plasma flow, it is turned less by the jet. These particles thus travel further in the z direction, resulting in the concave spray pattern. The particle velocity versus temperature relationship in Fig. 9(b) is analogous to that observed for turbulent dispersion, with tem-

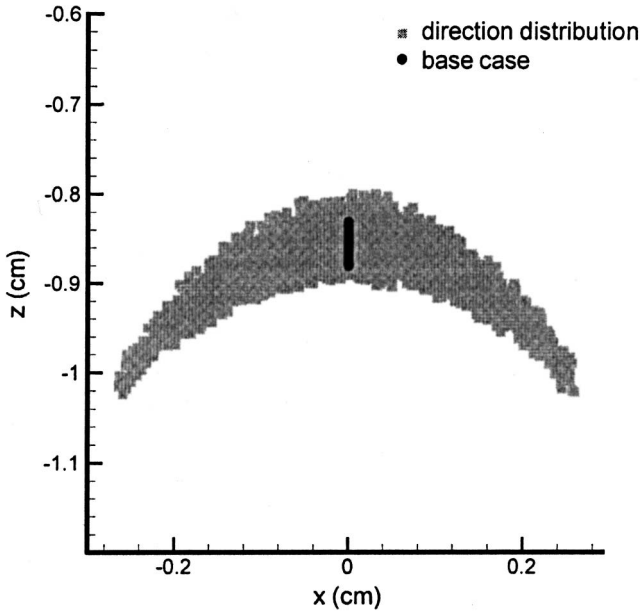

(a)

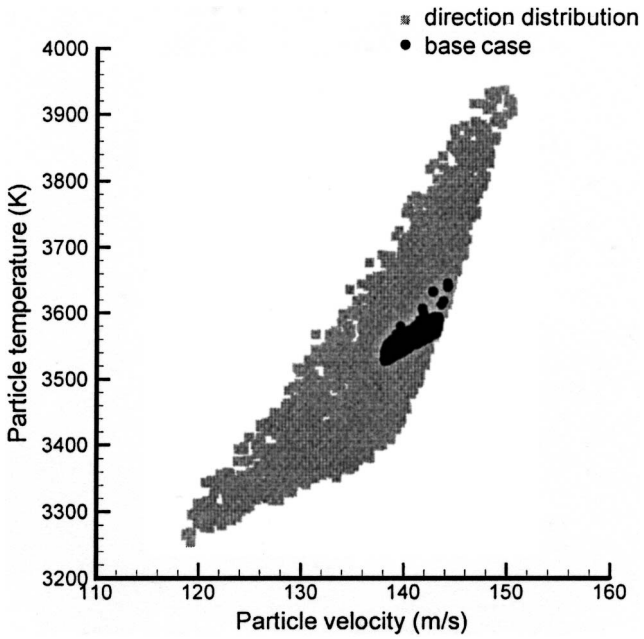

(b)

Fig. 9 The predicted **(a)** spray pattern and **(b)** particle velocity vs temperature relationship at 10 cm from the torch face, when a distribution in the particle injection direction (case 4) is included. Results from the base case calculation are also shown for comparison.

peratures reasonably well distributed above and below the base case but velocities generally lower.

4.5 Particle Size

Introducing a particle size distribution (i.e., case 5) results in a spray pattern very similar to that shown in Fig. 8(a) (no dispersion in x); however, the distribution is wider, varying between approximately 0 and −2.4 cm. Figure 10 shows the particle spatial position at 10 cm from the torch face plotted as a function of particle diameter. For identical injection velocities and direction, the larger particles tend to penetrate farther into the flow field while the smaller particles are more readily turned and swept downstream. Thus, aerodynamic sizing is an important aspect of the thermal spray process. Figure 11 shows the predicted particle velocity and temperature versus particle diameter relationships at 10 cm from the torch face, with results from the base case calculation again included for comparison. Both the velocity and temperature are significantly affected by particle size. As observed previously, the smallest particles are accelerated to the highest velocities (aerodynamic sizing). Note a peak in particle temperature at a diameter of approximately 25 μm. Particles smaller than this are easily turned by the plasma jet and never experience its high temperature core. Above this, the thermal mass of the particle restricts its temperature. The flat portion of the curve in Fig. 11(b) corresponds to the melting temperature of ZrO_2 (~2950 K), thus, particles having diameters between approximately 70 and 105 μm are predicted to be mixed phase and, above 105 μm, still solid at the deposition plane.

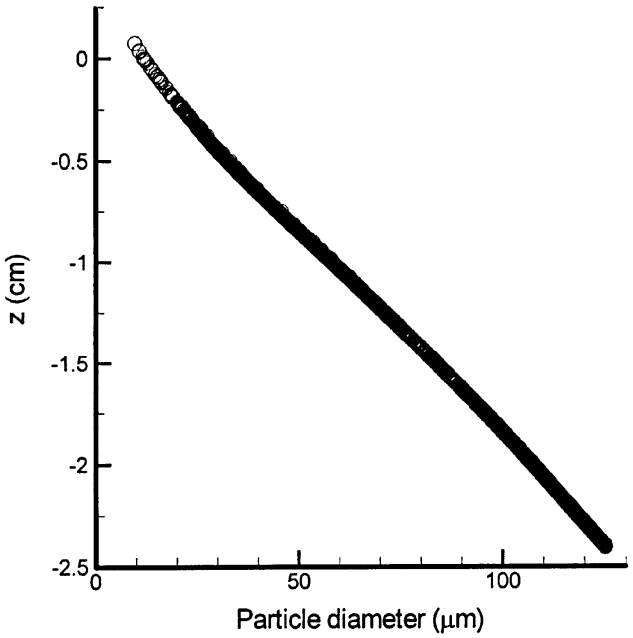

Fig. 10 The particle diameter vs spatial position at 10 cm from the torch face showing aerodynamic sizing, an important aspect of the thermal spray process

Note in Fig. 11 that the base-case particle velocity and temperature at a given particle size falls slightly below that predicted in this case, where the particle size was varied. This small discrepancy is due to the effect described previously, where all particles in the base case simulation follow essentially the same trajectory and result in slight local slowing and cooling of the plasma jet. As the particles become more dispersed, the coupling between the particles and the plasma jet becomes less important.

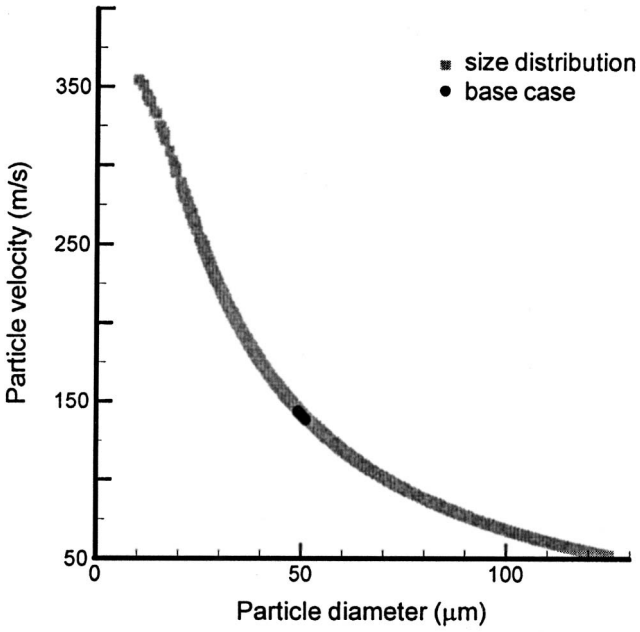

(a)

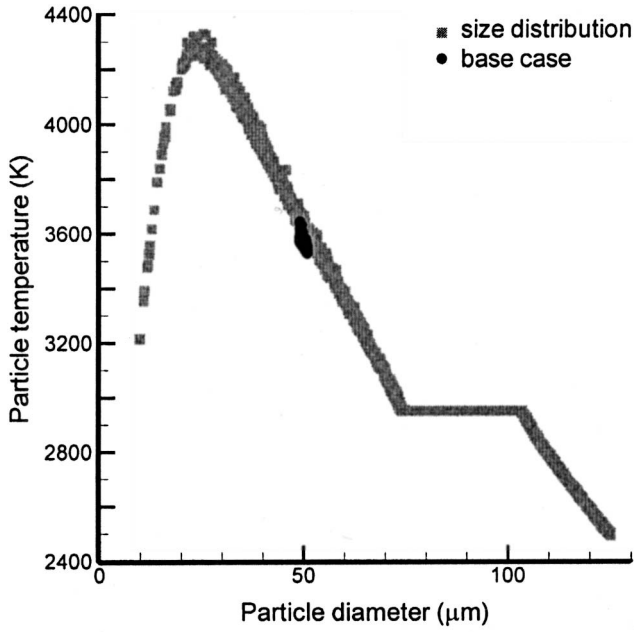

(b)

Fig. 11 The predicted **(a)** particle velocity and **(b)** particle temperature vs particle diameter relationships at 10 cm from the torch face (case 5). Results from the base case calculation are also shown for comparison.

4.6 Particle Density

The effects of including a particle density distribution (i.e., case 6) are illustrated in Fig. 12, which shows the predicted particle velocity versus temperature relationship at 10 cm from the torch face. The region of lowest temperature and velocity, where the two cases overlay, corresponds to the most dense particles. Lighter particles are more easily turned by the plasma jet and are accelerated to higher velocities. Even though the lighter particles traverse a cooler portion of the jet, they achieve higher temperatures due to a smaller thermal mass.

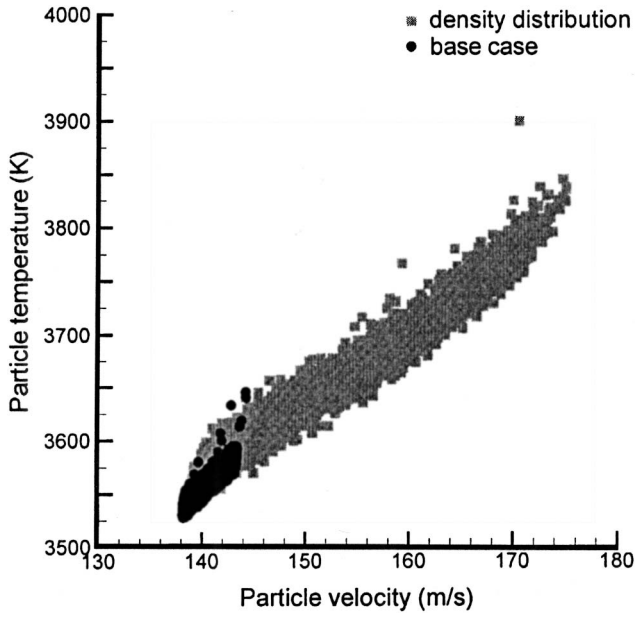

Fig. 12 The predicted particle velocity vs temperature relationship at 10 cm from the torch face, when a particle density distribution (case 6) is included. Results from the base case calculation are also shown for comparison.

4.7 Combined Effects

A comparison of the separate effects of the preceding simulations provides information on their relative influence, plus insight and guidance for the control and optimization of spray patterns and particle deposition conditions.

Consider, for example, Fig. 13, which shows the calculated spray patterns for cases 1 through 6, when each phenomenon is considered individually (Fig. 13a and b) and, then, the combined result (case 7), when all effects are considered simultaneously (Fig. 13c). As before, results are plotted for all particles passing through a plane 10 cm from the torch face. Figure 13(a) isolates those phenomena that affect particle dispersion in the injection direction only (particle density, size, and velocity). Note that because the results overlay and are difficult to compare graphically, the particle plots have been artificially separated a fixed distance. Figure 13(b) then isolates those phenomena that control particle dispersion both parallel and perpendicular to the injection direction (turbulence and cone angle). For the conditions considered in this study, dispersion in the injection direction (Δz) is most affected by particle size (~2.4 cm), followed by the injection velocity (~1.6 cm), and then turbulence (~0.6 cm). Particle density and cone angle appear to have a similar but smaller effect (~0.3 cm). The range of particle densities used (70 to 100% of fully dense material) is arbitrary as little data are available. Scanning electron microscopy (SEM) photographs of spray-dried and plasma-sintered (and spheridized) material suggest that the range of densities of some commercially available materials may be even greater than that assumed. The results suggest, however, that even if the density variation were greater

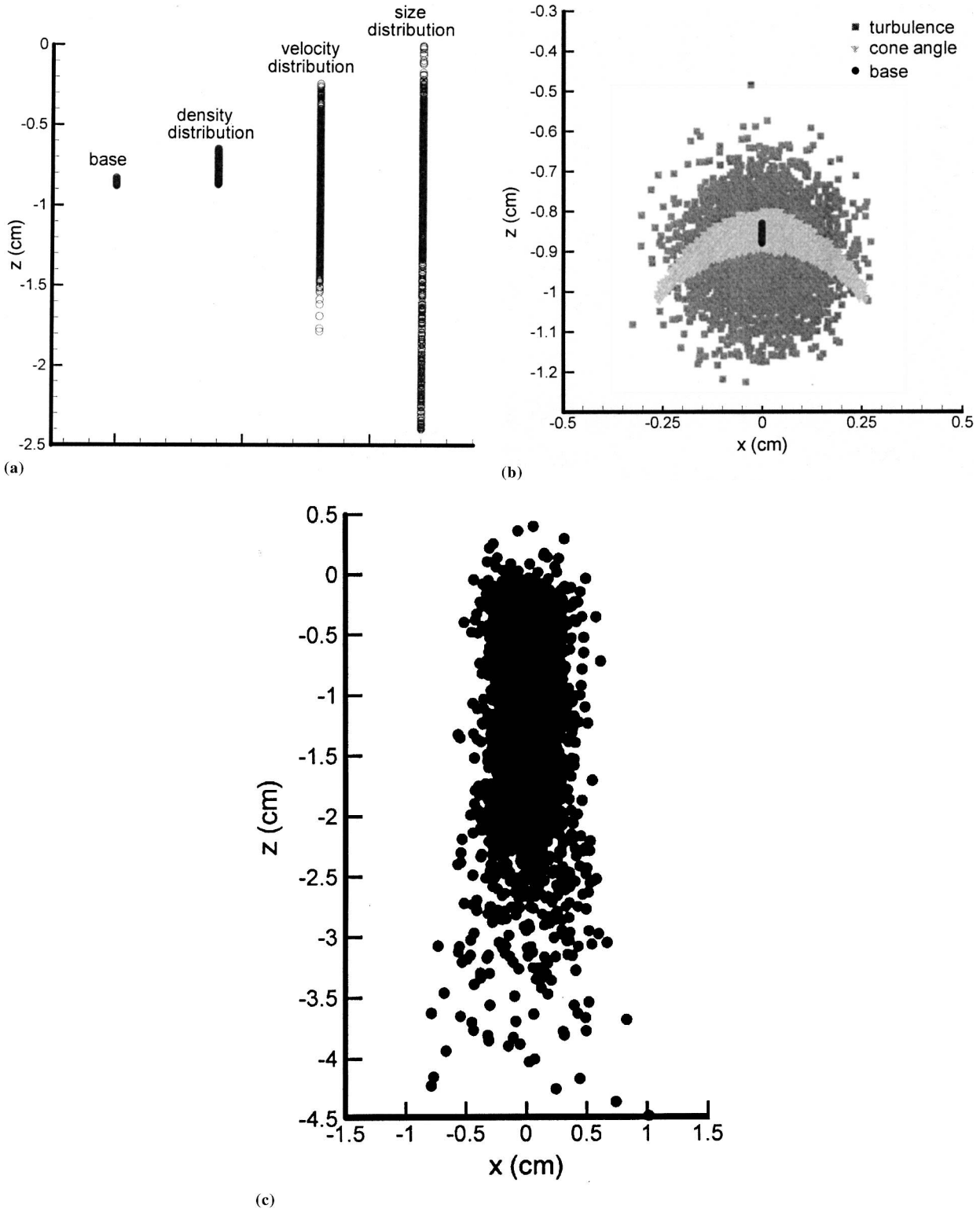

Fig. 13 The calculated spray patterns for cases 1 through 6, when each phenomenon is considered individually **(a)** and **(b),** and then the combined result, when all phenomena are considered simultaneously **(c).** Results are plotted for all particles passing through a plane 10 cm from the torch face.

by a factor of 2, the effect of velocity distribution and size distribution would still dominate.

Dispersion normal to the injection direction (Δx) appears to be similarly affected by turbulence and the assumed cone angle (~0.6 cm). The combined effect is a spray pattern that is roughly 3 × 1 cm, as shown in Fig. 13(c).

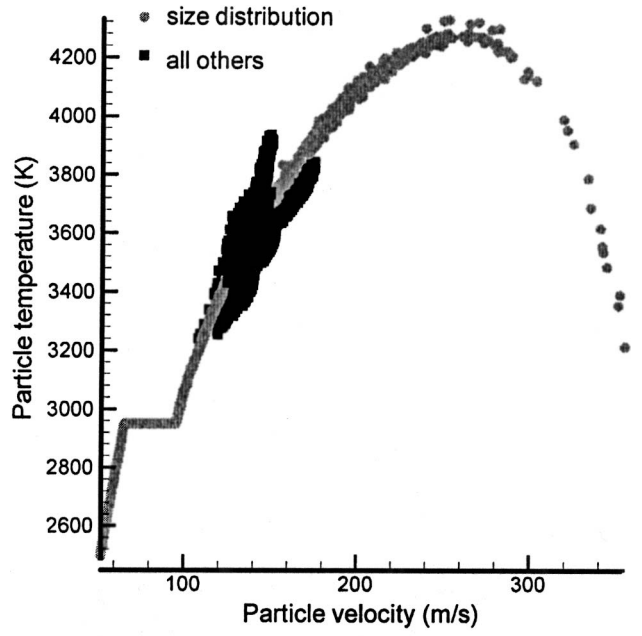

(a)

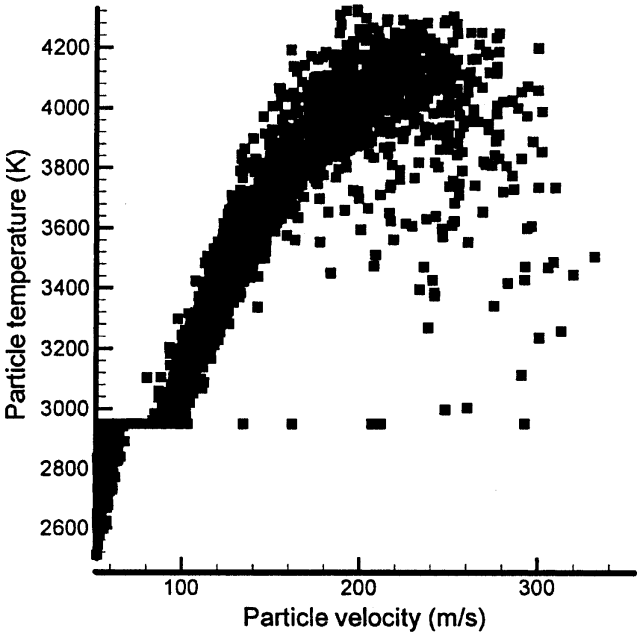

(b)

Fig. 14 The calculated particle velocity vs temperature relationships when each phenomenon is considered separately **(a)** and when all phenomena are considered simultaneously **(b).** In (a), the effects of turbulence and particle velocity, direction, and density are lumped together. Results are plotted for all particles passing through a plane 10 cm from the torch face.

A similar comparison of the particle velocity and temperature results is shown in Fig. 14. Data from the separate effect calculations (cases 1 through 6) are given in Fig. 14(a) and the combined results (case 7) in Fig. 14(b). In Fig. 14(a), the effects of turbulence and particle velocity, direction, and density are lumped together. Clearly, the particle size distribution has the dominant effect on particle velocity and temperature. Even in the combined results, the effects of particle size are obvious, with all other phenomena simply causing a widening of the distribution.

5. Conclusions

Using computational modeling, a systematic study has been performed to investigate various particle-related phenomena affecting plasma spray coatings. Investigating each phenomenon separately provides valuable insight into particle behavior.

For the typical plasma jet and injection conditions considered, particle dispersion in the injection direction is most significantly affected by (in order of decreasing importance): particle size distribution, injection velocity distribution, turbulence, and injection direction distribution or particle density distribution. Only the distribution of injection directions and turbulence affect dispersion in the normal direction and are of similar magnitude in this study. With regards to particle velocity and temperature, particle size is the dominant effect.

Acknowledgments

This work was performed under the auspices of the U.S. Department of Energy under DOE Field Office, Idaho, Contract No. DE-AC07-99ID13727, supported by the U.S. Department of Energy, Office of Science, Office of Basic Energy Sciences, Division of Engineering and Geosciences.

References

1. L. Pawlowski: *The Science and Engineering of Thermal Spray Coatings*, Wiley, New York, NY, 1995.
2. "Thermal Spraying, Current Status and Future Trends," *Proc. 14th Int. Thermal Spray Conf*., A. Ohmori, ed., High Temperature Society of Japan, Osaka, 1995.
3. *Thermal Spray: Practical Solutions for Engineering Problems*, C.C. Berndt, ed., ASM International, Materials Park, OH, 1996.
4. *Thermal Spray: A United Forum for Scientific and Technological Advances*, C.C. Berndt, ed., ASM International, Materials Park, OH, 1997.
5. A. Vardelle, P. Fauchais, B. Dussoubs, and N.J. Themelis: *Plasma Chem. Plasma Processing,* 1998, *18,* pp. 551-74.
6. R. McPherson: *Thin Solid Films,* 1981, *83,* pp. 297-310.
7. P. Fauchais, A. Vardelle, M. Vardelle, L. Bianchi, and A.C. Leger: *Plasma Chem. Plasma Processing,* 1996, *16,* pp. 99S-126S.
8. L. Bianchi, A. Grimaud, F. Blein, P. Lucchese, and P. Fauchais: *J. Thermal Spray Technol*., 1995, *4,* pp. 59-66.
9. J.K. Dukowicz: *J. Comput. Phys*., 1980, *35,* pp. 229-53.
10. P.J. O'Rourke: *J. Comput. Phys*., 1989, *83,* pp. 345-60.
11. A.A. Amsden, J.D. Ramshaw, P.J. O'Rourke, and J.K. Dukowicz: "KIVA: A Computer Program for Two- and Three-Dimensional Fluid Flows with Chemical Reactions and Fuel Sprays," Los Alamos National Laboratory Report No. LA-10245-MS*,* Los Alamos National Laboratory, Los Alamos, NM, 1985.
12. J.D. Ramshaw and C.H. Chang: *Plasma Chem. Plasma Processing,* 1992, *12,* pp. 299-325.
13. C.H. Chang and J.D. Ramshaw: *Phys. Plasmas,* 1994, *1,* pp. 3698-708.
14. Y.P. Wan, V. Prasad, G.-X. Wang, S. Sampath, and J.R. Fincke: *Proc. ASME Heat Transfer Division*, R.A. Nelson, ed., ASME, New York, NY, 1998, *4,* pp. 66-77.

15. C.H. Chang: *Thermal Spray: International Advances in Coatings Technology,* ASM International, Materials Park, OH, 1992, pp. 793-98.
16. B. Dussoubs: Ph.D. Dissertation, Universite de Limoges, Limoges, France, 1998.
17. J.R. Fincke, W.D. Swank, and D.C. Haggard: in *Thermal Spray: Surface Engineering via Applied Research*, C.C. Berndt, ed., ASM International, Materials Park, OH, 2000, pp. 9-14.
18. S. Snyder, L. Reynolds, G. Lassahn, J. Fincke, and C. Shaw: *Phys. Rev. E.*, 1993, *47,* pp. 1996-2005.
19. J.R. Fincke, C.H. Chang, W.D. Swank, and D.C. Haggard: *Int. J. Heat Mass Transfer*, 1994, *37*(11), pp. 1673-82.
20. M.A. Leschziner and W. Rodi: *AIAA J.*, 1984, *22*(12), pp. 1742-47.
21. J.R. Fincke, W. Swank, and D. Haggard: in *Thermal Spray: United Forum for Scientific and Technological Advances*, C.C. Berndt, ed., ASM International, Materials Park, OH, 1997, pp. 335-42.